Organic & Biomolecular Chemistry

Cite this: *Org. Biomol. Chem.*, 2011, **9**, 5162

www.rsc.org/obc

PAPER

Theoretical studies on the inactivation mechanism of γ-aminobutyric acid aminotransferase

A. T. Durak, H. Gökcan and F. A. S. Konuklar*

Received 27th January 2011, Accepted 15th April 2011
DOI: 10.1039/c1ob05146f

The inactivation mechanism of γ-aminobutyric acid aminotransferase (GABA-AT) in the presence of γ-vinyl-aminobutyric acid, an anti-epilepsy drug, has been studied by means of theoretical calculations. Density functional theory methods have been applied to compare the three experimentally proposed inactivation mechanisms (Silverman *et al.*, *J. Biol. Chem.*, 2004, **279**, 363). All the calculations were performed at the B3LYP/6-31+G(d,p) level of theory. Single point solvent calculations were carried out in water, by means of an integral equation formalism-polarizable continuum model (IEFPCM) at the B3LYP/6-31+G(d,p) level of theory. The present calculations provide an insight into the mechanistic preferences of the inactivation reaction of GABA-AT. The results also allow us to elucidate the key factors behind the mechanistic preferences. The computations also confirm the importance of explicit water molecules around the reacting center in the proton transfer steps.

Introduction

γ-Aminobutyric acid aminotransferase (GABA-AT) is a pyridoxal 5′-phosphate (PLP) dependent enzyme responsible for the degradation of the primary inhibitory neurotransmitter γ-Aminobutyric acid (GABA) into succinic semialdehyde and L-glutamate.[1] GABA-AT consists of two identical homodimers, and coenzyme PLP forms a Schiff base with the ε-amino group of Lys-329 on each monomer.

Due to its crucial role in interneural communication, maintaining a certain level of GABA concentration in the brain is of vital importance. When the brain's GABA concentration drops below the critical threshold, convulsions occur, which lead to several other neurological diseases such as Parkinson's disease and Alzheimer's disease.[2,3]

External (oral or intravenal) GABA introduction has proven ineffective, as GABA, under normal conditions, cannot cross the blood-brain barrier.[4] Using an inhibitor that can cross the blood-brain barrier and intervene in GABA metabolism by reacting with relevant enzymes is a method of increasing the GABA level. GABA-AT has been shown to be a valid target for such an attempt: an anticonvulsant drug may selectively inhibit or inactivate GABA-AT, thereby causing a buildup of GABA.[5]

To facilitate selectivity, many drugs exhibiting a GABA backbone have been proposed and many of them exhibited anticonvulsant properties.[6–10] Research for more potent drugs is ongoing, and over the years, relatively more potent drugs have been designed. Among mechanism-based GABA-AT inhibitors, the 4-amino-5-hexenoic acid also known as γ-vinyl-GABA is the most common drug in use.[6,11]

γ-vinyl-GABA has been observed to be successful in some epilepsy cases where other drugs have failed.[12] Furthermore, experiments on mice and monkeys promise a role in drug addiction treatment.[13] γ-vinyl-GABA has been an approved drug in the market for over 25 years and no lethal effects have been observed. The most severe effect to date was a decrease in field of vision in children after prolonged use.[14] The effects of the inactive R-isomer are unexplored, and the drug is sold as a racemic mixture. γ-vinyl-GABA has a single chiral center and exhibits high elasticity. The presence of carboxylic and amino groups allows strong intra and intermolecular hydrogen bonds. In addition to experimental studies based on its structural properties, conformational analysis for γ-vinyl-GABA has been performed by means of the Hartree Fock method, using the 6-311++G** basis set and possible hydrogen bonds calculated *via* the AIM (Atoms in Molecules) method by Sadlej-Sosnowska *et al.*[15]

The inactivation mechanism of GABA-AT in the presence of γ-vinyl-GABA has been investigated in experimental studies, based on various methods such as spectroscopic and radiolabeling studies,[16] radiochemical methods,[17] and occasionally using chemical intuition.[18] Based on these studies, three different reaction mechanisms were proposed. The Michael addition pathway was first suggested by Lippert *et al.*[11] The data obtained from ^{14}C labeling experiments, however, support the Enamine-Michael addition mechanism, resulting in a different product than Michael addition pathway.[16]

Nanavati *et al.*[17] observed the product of the Enamine mechanism (Scheme 1), which is found to be a minor product having a formation ratio of 25 : 75 with respect to the Michael Addition pathway product. X-ray crystallography data,[19] based

Istanbul Technical University Informatics Institute, Computational Science and Engineering Programme Ayazağa Campus, 34469, Maslak, Istanbul, Turkey. E-mail: konuklar@itu.edu.tr; Fax: +90 212 2857073

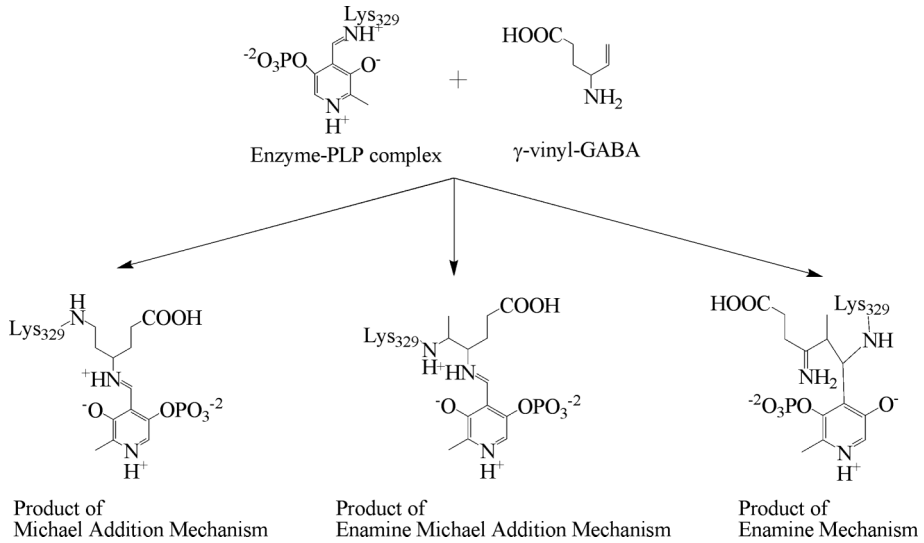

Scheme 1 The schematic representation of GABA-AT, γ-vinyl-GABA and the products obtained depending on the type of inactivation mechanism.

on the electron density, pointed out the formation of the Michael Addition product (Scheme 1).

Nevertheless, the experimental findings are insufficient to reveal the exact inactivation mechanism of GABA-AT. The present work is a comprehensive density functional theory (DFT) study conducted at the B3LYP/6-31+G(d,p) level of theory[20] on the inactivation mechanism of GABA-AT. The work presented here will be the first attempt to investigate the details of the inactivation mechanism of GABA-AT theoretically. The three inactivation mechanisms described in Silverman's paper[19] – Michael Addition, Enamine-Michael Addition and Enamine mechanisms – are examined by means of DFT calculations. The calculated results provide a detailed energetic profile for the inactivation mechanism of GABA-AT. The role of explicit water molecules during the proton transfer steps is also investigated. The comparison of energy profiles along with the geometries, charge densities of the intermediate and transition state structures enabled us to describe the preferred reaction mechanism in detail.

Computational details

The conformer search for both the PLP-enzyme complex and γ-vinyl-GABA were performed at the semiempirical level of theory using the PM3[21] hamiltonian included in the Spartan'04 program package.[22] Conformers with lowest energies were then subjected to geometry optimizations and frequency calculations, at B3LYP/6-31+G(d,p) level of theory which is implemented in the Gaussian '03 package of programs.[23]

All geometries involved in the reaction path have been fully optimized at the at the B3LYP/6-31+G(d,p) level of theory, which is known to perform reasonably well in the prediction of geometries. The polarization functions on the hydrogen atoms were used to provide more accurate descriptions, particularly for the proton transfer steps. The free energy values obtained from the gas phase calculations include thermal free energy corrections at 298 K and 1 atm.

Vibrational analyses were carried out on the optimized structures to characterize minima and saddle points. Additionally, Intrinsic Reaction Coordinate (IRC) calculations were performed for further characterization of the transition states. Relative free energies of activation ($\Delta G^{\neq}$) are calculated as the difference of free energies between transition states and reactants of each step.

Natural Bond Orbital (NBO) analysis was performed in order to figure out the importance of stereo-electronic effects on the stability of the structures along the reaction path.[24] The solvation effect of water has been considered by B3LYP/6-31+G(d,p) single point calculations on the optimized gas-phase geometries using the polarizable continuum model (PCM) of the Tomasi's group.[25] By default, Gaussian 03 uses a standard state of 1 atm. However, conventionally, in solution phase calculations a standard state of 1 M is used for solutes and 55.55 M for water (the concentration of pure water). Therefore, a correction term accounting for the change from the gas-phase standard state to solution standard state of 1 M is added to the free energies of solutes (1.89 kcal mol^{-1} at 298.15 K). The single point MP2 calculations on the optimized structures were also performed with the same basis set 6-31+G(d,p). The MP2 energies are given in the Supporting Information section. The MP2 energies are in qualitative agreement with results obtained at the B3LYP levels of theory.

In calculations, methylamine is used as a model structure to mimic the Lysine 329. In addition, the phosphate group on PLP is replaced by a methyl group. These techniques are common and widely used in the quantum mechanical calculations of the PLP-dependent enzyme reaction mechanisms.[26–30]

The experimental findings have shown that the carboxyl end of γ-vinyl-GABA is held at a fixed geometry by the side chain of Arginine (Arg192).[19] In order to reduce polarity on the carboxyl end and to prevent negatively charged oxygen atoms from twisting γ-vinyl-GABA upon itself, the oxygen on the carboxyl end was protonated.

While previous publications on PLP-dependent enzymes do not attribute any active role to the pyridine ring in reaction mechanisms, the same cannot be said about imine nitrogen on the ring. In the study, the model structure representing the PLP-enzyme complex is chosen to be ketoenamine type. Therefore

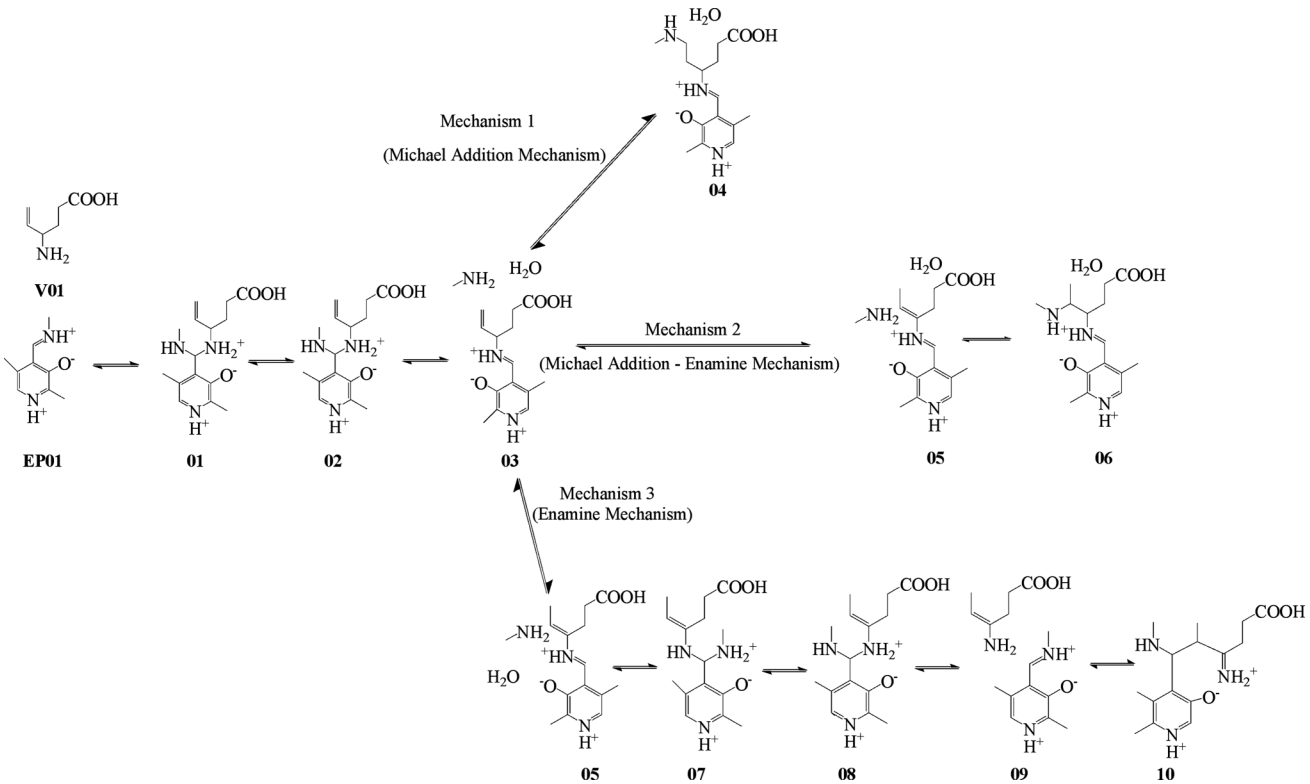

Scheme 2 Proposed inactivation mechanisms of GABA-AT in the presence of γ-vinyl GABA. *Mechanism 1*: Michael Addition, *Mechanism 2*: Enamine Michael Addition, *Mechanism 3*: Enamine Mechanism.

the imine nitrogen on PLP ring was protonated to decrease the charge delocalization on the pyridine moeity.[27–32] The graphical representations were obtained using the CYLview program.[33]

Results and discussion

The details of the proposed mechanisms for the inactivation of GABA-AT in the presence of γ-vinyl-GABA are presented in Scheme 2. The internal aldimine, a PLP Schiff base with an amino group of Lys329 residue, is converted to the external aldimine, a new PLP Schiff base with the γ-vinyl-GABA. In literature, the external aldimine formation is also known as transimination.[26,29–32] After the formation of external aldimine, three different pathways have been proposed for the inactivation. The first one is the Michael Addition, which simply involves the nucleophilic attack on the carbon-carbon double bond. The Enamine-Michael addition involves allylic isomerization through a carbon-carbon double bond that is followed by the Michael addition. The last mechanism is known as the Enamine pathway, in which the methylamine attaches to the PLP imine carbon, leading to the formation of enamine (**09**). The mechanism ends up with the attack of enamine to PLP imine to give the enamine adduct.

For the determination of reactants, initial structures are examined *via* systematic conformer analysis with 3-fold rotation around the single bonds using the semiemprical PM3 method. The obtained conformers are then subjected to a further optimization at the B3LYP/6-31+G** level of theory.

The energy difference between the conformers of γ-vinyl-GABA is relatively small (Table 1). The conformer proposed by Sadlej-Sosnowska *et al.*[15] as having the lowest energy, according to the HF method utilizing the 6-311+G** basis set, was also taken into consideration during the conformer analysis. This conformer (**V05**) is found to have 1.1 kcal mol^{-1} higher free energy than **V01** when the calculations are carried out at the B3LYP/6-31+G(d,p) level of theory. The energy difference between two lowest energy conformers of the Enzyme-PLP complex, which is mimicked with Methylamine-PLP complex throughout the study, is found to be 11.3 kcal mol^{-1}.

Table 1 Relative energies (in kcal mol^{-1}) for the conformers of γ-vinyl-GABA,computed at B3LYP/6-31+G** level of theory

	Relative energies (kcal mol^{-1})	
	Gas phase[a]	SCRF-IEFPCM[b]
V01	0.0	0.0
V02	0.5	1.0
V03	0.6	0.0
V04	0.9	0.6
V05	1.1	3.7
V06	2.0	0.9

[a] Relative free energies (in kcal mol^{-1}) in gas phase. [b] Relative energies (in kcal mol^{-1}) calculated in water.

External aldimine formation

The external aldimine formation consists of several steps. The free energy profile of the external aldimine formation is depicted in Fig. 1. The reaction starts with the nucleophilic attack of N19 on substrate to C8 of the Methylamine-PLP complex. The

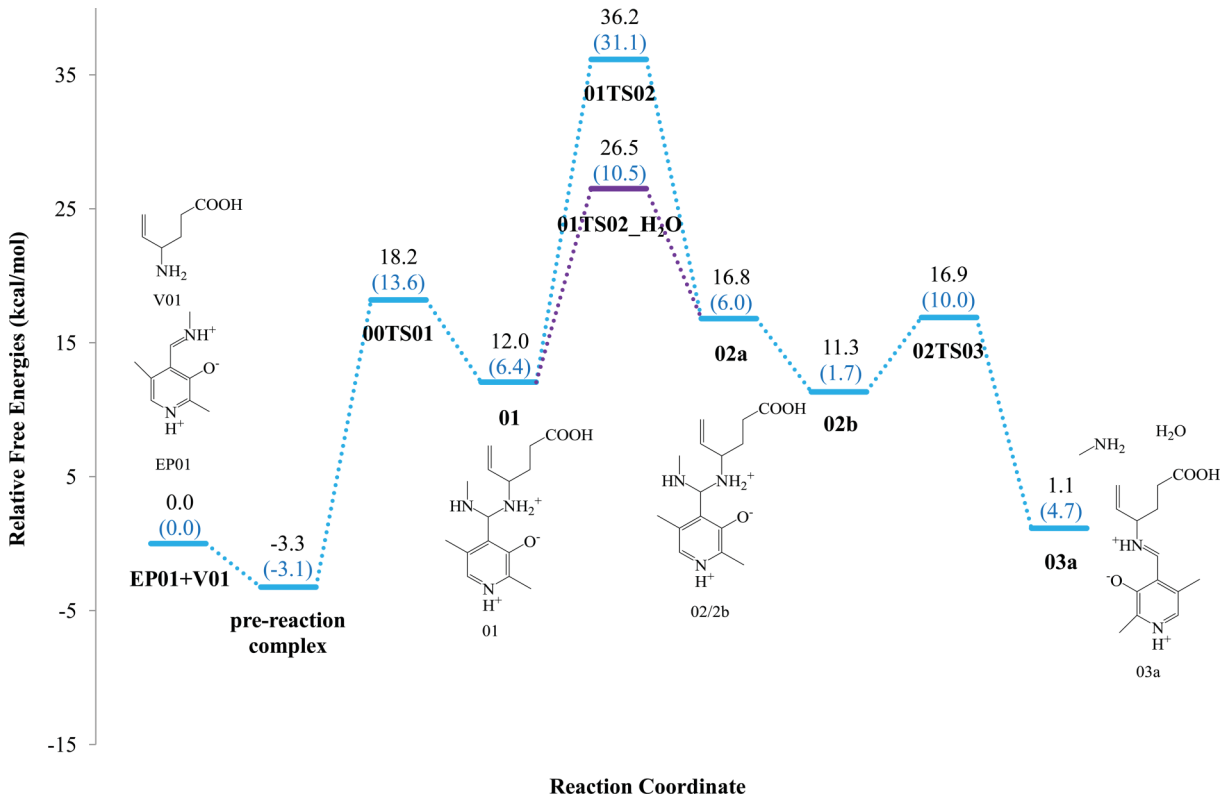

Fig. 1 The reaction profile for the External Aldimine Formation in gas phase calculated at B3LYP/6-31+G(d,p) level. Values in parantheses refer to the single point relative energies at the $PCM_{(water)}$/B3LYP/6-31+G(d,p) level of theory.

nucleophilic attack is accomplished through the transition state structure **00TS01**, in which the N19–C8 distance is 1.970 Å (Fig. 2). In structure **00TS01**, the presence of long range interactions between one of the hydrogen atoms on N19 and oxygen atom (O7) on the PLP ring (2.124 Å) and one of the hydrogen atoms on N9 with the same oxygen atom (2.174 Å) facilitate the formation of transition state structure **00TS01**. The gas phase energy barrier for the formation of intermediate structure **01** is calculated to be 18.2 kcal mol^{-1} (Fig. 1).

The second step in the external aldimine formation is the 1,3 proton transfer that is achieved *via* the six-centered ring transition state structure, **01TS02_H_2O**, in the presence of an explicit water molecule. In structure **01TS02_H_2O**, the N19–C13 and N9–C10 bonds are observed to stand symmetrically around the PLP ring (Fig. 2). The PLP ring keeps a perpendicular orientation relative to the amine groups of the methylamine and the γ-vinyl-GABA. The distances between O7 and the hydrogens on N9 and N19 are 2.056 Å and 2.115 respectively favoring a strong stabilizing interaction. Although the two intermediate structures, **01** and **02a**, resemble each other geometrically, the energy difference is found to be 4.8 kcal mol^{-1} (Fig. 1). The activation energy barrier is equal to 24.2 kcal mol^{-1} in the absence of an explicit water molecule. However, with the assistance of an explicit water molecule, the barrier is lowered by 9.7 kcal mol^{-1} (Fig. 1). Previous computational studies in the literature suggest that the addition of explicit water molecules to the reaction paths concerning proton transfers facilitates the transfers by shortening the distance protons have to travel and, in effect, lowering the energy barrier.[31a,32a,34]

Structure **02a** isomerizes into structure **02b**. The relative free energy of structure **02b** is 5.5 kcal mol^{-1} lower than that of structure **02a**, which is compatible with the intermediate structure **01**(Fig. 1). The interaction between one of the bonding orbitals of C11–C12 alkene bond and antibonding orbital of N9–H bond give an extra stabilization of about 5.60 kcal mol^{-1} to **02b** as compared to **02a**. In addition, the lone pair orbitals on atom O7 in structure **02b** are strongly coupled with N9–H. A detailed list of donor–acceptor interactions and their stabilization energies are given in the Supporting Information.

Despite the reversed direction of reaction and swapped location of involved parts, the transition between structures **02b** and **03a** (**02TS03**) is very similar to the transition state **00TS01** (Fig. 2). Using the hydrogen it received from γ-vinyl-GABA in the previous step, the methylamine has become stable and ready to leave the complex (Structure **02b**). The shortening in C13–N19 bond length to 1.336 Å and NBO results indicate the loss of the sp^3 hybridization scheme on atom N19.

In the obtained Schiff base, **03a**, the distance between the hydrogen on N19 and O7 on the PLP ring is 1.717 Å, and the value of N19–H–O7 angle is 128° where both indicate the presence of a stabilizing long range interaction (Fig. 2). In PLP complexes (**EP01** and **03**), the PLP ring is coplanar with the amino groups on C8. It prefers conformations that maximize the interaction of lone pairs of O7 with the hydrogens on nitrogen atoms of either methylamine or γ-vinyl-GABA. Thus, the external aldimine formation is completed with the formation of the substrate-PLP complex, with an energy barrier of 5.6 kcal mol^{-1}. The gas phase calculations revealed that the rate limiting is 1,3 proton transfer

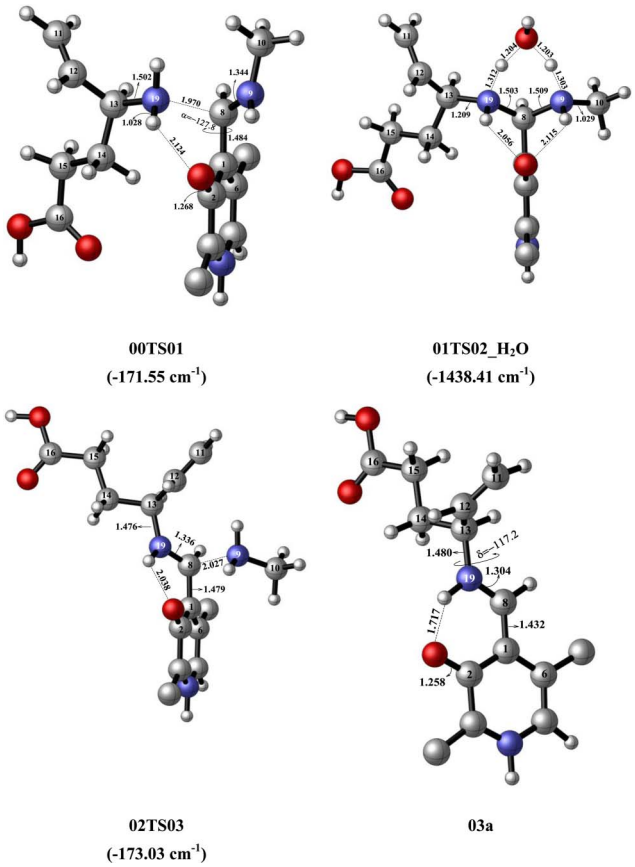

Fig. 2 Three dimensional representations of the stationary points for the External Aldimine Formation path.

step both in the absence and in the presence of an explicit water molecule. However, when the solvent effect is included, the first step, which involves the nucleophilic attack of γ-vinyl-GABA to Methylamine-PLP complex is found to be the rate limiting step.

Michael Addition pathway

1,2 Michael Addition reaction consists of the nucleophilic attack of neutral amine to the activated carbon-carbon double bond. In our model, the reaction involves the nucleophilic attack of the methylamine nitrogen (N9) on the C11 of the alkene group in the PLP-substrate complex and a transfer of the proton to the C12 of the alkene group (Scheme 2).

The Michael addition reaction may also occur with the assistance of an explicit solvent molecule.[34–37] The presence of a water molecule is capable of lowering the energy barrier of the reaction, as well as altering the structure of the product. The gas phase calculations have revealed that the Michael addition mechanism must overcome a barrier of 48.2 kcal mol^{-1} in the absence of water assistance; however, in the presence of water assistance, the barrier is lowered to 40.7 kcal mol^{-1}. (Fig. 3). Furthermore, single point solvent effect calculations decreased the barrier to 14.8 kcal mol^{-1}, which is in keeping with the previous theoretical findings.[28,31,35,36] The presence of explicit water molecules and the solvent environment facilitate the Michael Addition mechanism. A previous computational study on the Michael addition reaction has analyzed the nucleophilic attack of the ammonia molecule on a carbon-carbon double bond at the MP2/6-31G* level of theory.[35] The study used water as a proton bridge and determined the activation barrier to be 22.9 kcal mol^{-1} high. In our work, gas phase single point MP2/6-31+(d,p) calculations reduced the barrier up to 35.0 kcal mol^{-1}.

The presence of the water molecule has also affected the geometries of the transition states and the product formed. The cartesian

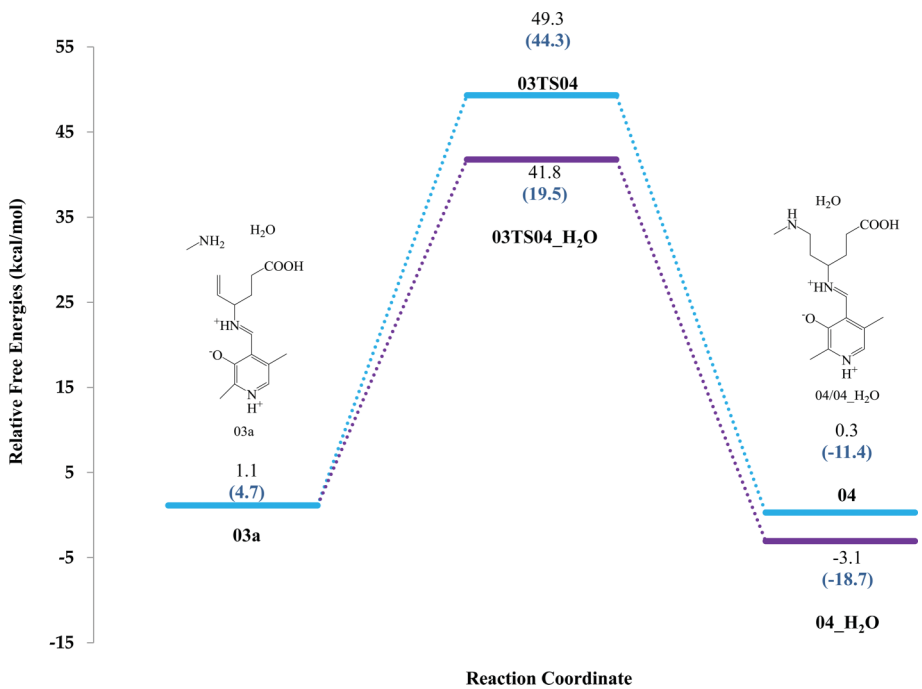

Fig. 3 The reaction profile for the Michael addition (Mechanism 1) in gas phase calculated at B3LYP/6-31+G(d,p) level. Values in parantheses refer to the single point relative energies at the PCM$_{(water)}$/B3LYP/6-31+G(d,p) level of theory.

coordinates of the unassisted geometries of transition states and products formed are given in the Supporting information.

Both in the water assisted and unassisted pathways, during the nucleophilic attack of methylamine, pyramidalization is observed on atoms C11 and C12. It should be pointed out that a charge separation for atoms C11 and C12 is observed in structure **03TS04_H$_2$O** (Fig. 4). The proton transfer is facilitated with the pyramidalization and charge alterations on atom C12. Based on the results obtained, the reaction can be classified as asynchronous and concerted where the proton transfer is facilitated with the nucleophilic attack.

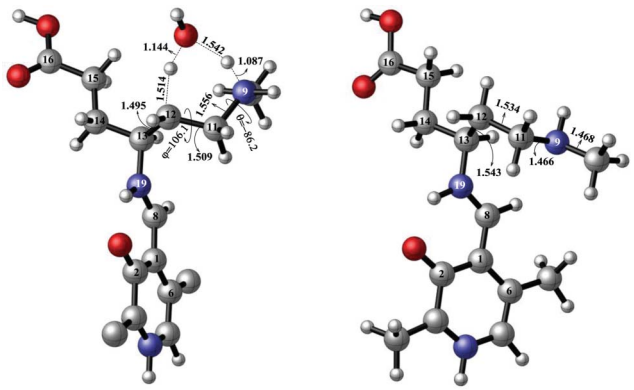

Fig. 4 Three dimensional representations of the stationary points for the Michael Addition Path (Mechanism 1).

The water assistance in the Micheal addition step yields a different product (Structure **04_H$_2$O**) being 3.4 kcal mol^{-1} lower in energy than the product obtained in the unassisted path (Fig. 3).

It is also noteworthy to state that the three-dimensional structure of the product obtained from the water-assisted reaction presents a better agreement with the structure proposed in experimental X-ray crystallographic studies (Fig. 4).[19]

Enamine-Michael Addition pathway

The Enamine-Michael Addition mechanism was proposed as an alternative to the Michael addition mechanism. The reaction starts with an allylic isomerization leading to the formation of enamine intermediate. The mechanism proceeds with the Michael addition reaction the methylamine to the alkene bond (Scheme 2). The steric hindrance around the C12 carbon atom prevents the usage of water assistance in the allylic isomerization step. A less hindered isomer is required to facilitate the water assistance. A less hindered isomer is obtained *via* rotation around dihedral angle (δ) (Fig. 2). The energy difference between two isomers is 1.3 kcal mol^{-1} (Fig. 5). As the structure **03a** isomerizes to **03b**, the electrophilicity of the hydrogen on C13 increases (qH13 = 0.253 in **3a**, qH13 = 0.275 in **3b**) where the charge on C12 remains relatively unchanged (Fig. 6).

The allylic isomerization can be modeled *via* a six-membered transition state structure, using only one explicit water molecule, or in the presence of two explicit water molecules (Fig. 6). The energy barrier is highly affected by the addition of an extra water molecule, as the barrier height is decreased by 12.7 kcal mol^{-1} (Fig. 5). Two different forms of the product are obtained from the two different transtition state structures. The product obtained from **03TS05_2H$_2$O**, **05b**, is energetically more favorable relative

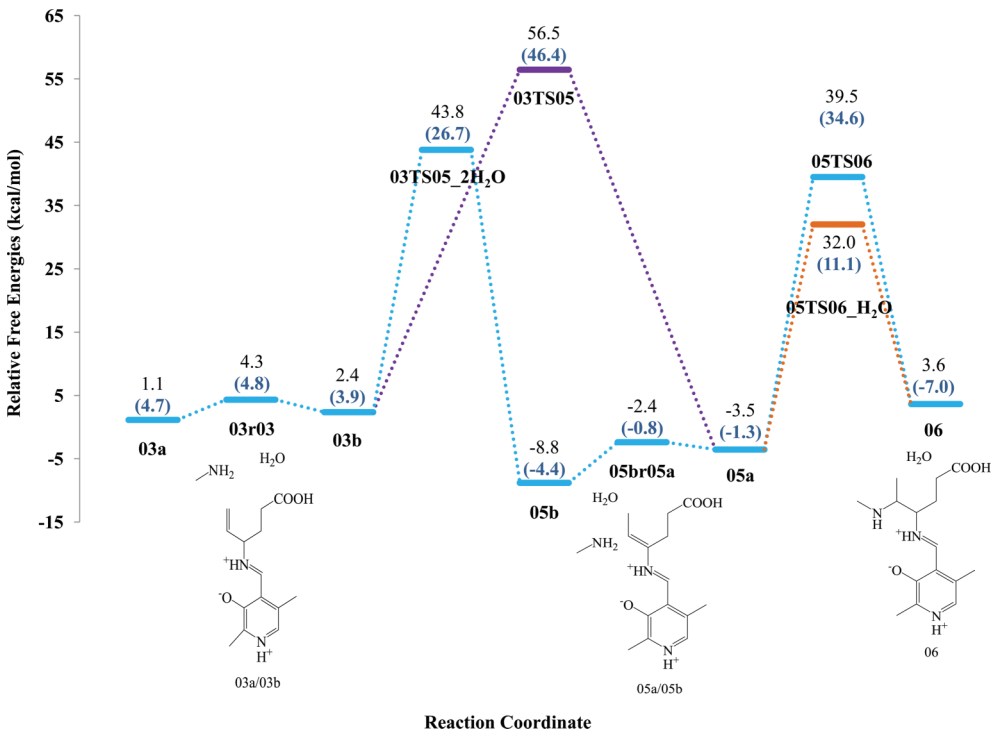

Fig. 5 The reaction profile for the for Enamine-Michael Addition (Mechanism 2) in gas phase calculated at B3LYP/6-31+G(d,p) level. Values in parantheses refer to the single point relative energies at the PCM$_{(water)}$/B3LYP/6-31+G(d,p) level of theory.

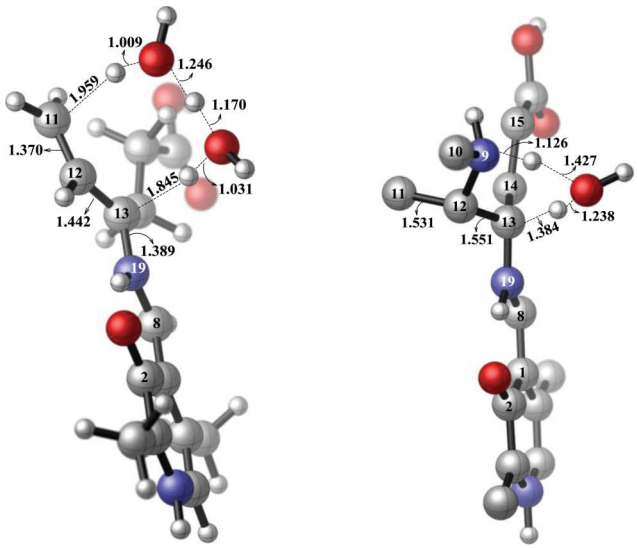

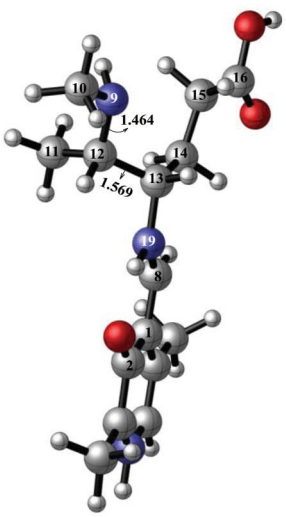

Fig. 6 Three dimensional representations of the stationary points for the Enamine-Michael Addition path (Mechanism 2).

to **05a**. The energy difference between two conformers is 5.4 kcal mol^{-1}. The structure **5a** is obtained with a rotational transition state (**05br05a**) having an energy barrier of 6.4 kcal mol^{-1} (Fig. 5).

The Michael addition step, which completes the inactivation, involves the nucleophilic attack of methylamine on the C12 of the alkene bond. This addition can occur with or without the assistance of a water molecule, as in the previous Michael addition mechanism. Thus, combined with the facilitation of proton transfers, the presence of water lowers the activation energy barrier from 43.0 kcal mol^{-1} to 35.5 kcal mol^{-1} (Fig. 5) in gas phase calculations.

Unlike the Michael addition pathway, both unassisted (**05TS06**) and water assisted (**05TS06_H$_2$O**) transition states lead to the formation of the same product, **06** (Fig. 5). The reaction is endergonic. The relative free energy of the product **06** is 3.6 kcal mol^{-1}. It should be noted that the obtained product after the Enamine-Michael addition mechanism is less stable than the product obtained at the end of the Michael addition pathway.

Enamine pathway

The alternative route to Michael Addition and Enamine Michael addition pathways was named the Enamine mechanism by the experimentalists.[16] Enamine mechanism starts with the same allylic isomerization step as the Enamine-Michael addition path (Fig. 7). In order to lead to the formation of enamine Schiff base adduct with PLP, the reaction must be proceed with the active site lysine mediated transimination to give the enamine and lysine bound PLP.[38,39] If the enamine is confined to a proper conformation, it can undergo nucleophilic addition to the lysine-bound PLP.

The mechanism continues with the attack of methylamine on the PLP imine carbon which is modeled with the transition state structure, **05TS07** (Fig. 8). The transition state structure is stabilized energetically by the long-range interactions between O7 and the hydrogens on N9 and N19 (Fig. 8). The stabilizing effect of long range interactions is also validated with NBO second order perturbative estimates of donor–acceptor interactions. Furthermore, the hyperconjugative interactions between the lone pair of N9 and the antibonding orbital of the N19–C8 bond has a value of 95.64 kcal mol^{-1}. The activation energy barrier of the first step is found to be 17.0 kcal mol^{-1} in gas phase, and the reaction ended up with the formation of intermediate **07**, as shown in Fig. 7. The structure, **07**, the hydrogen atoms on N9 are closer to the O7 and O17, pointing out stronger hyperconjugative interactions: the O17–H and O7–H distances become 1.997 Å and 1.657 Å respectively.

The reaction proceeds with a proton transfer from N9 to N19. The reaction occurs either in the presence or absence of an expilicit water molecule as in the External Aldimine formation part. In the water-assisted transition state, the transferred proton lies at 1.290 Å and 1.301 Å distances to N19 and N9 respectively (Fig. 8). These values are comparable to those for corresponding distances in structure **01TS02** (1.312 Å and 1.303 Å, respectively) (Fig. 2). The energy barrier to overcome for an assisted proton transfer is calculated to be 18.4 kcal mol^{-1}. which is 4 kcal mol^{-1} higher than the corresponding step in External Aldimine Formation. This difference can be explained by the reactant stabilities. The stabilizing interactions within the intermediate **07** is stronger than the intermediate **01**. After the allylic isomerization step, proton transfer represents the second highest energy barrier in the Enamine pathway.

The 1,3 proton transfer step is completed with the formation of intermediate **08a**, which then isomerizes into **08b** barrierless (Fig. 7). Following the **08a–08b** isomerization, γ-vinyl-GABA becomes ready to leave the complex by overcoming a 2.6 kcal mol^{-1} high barrier (Fig. 7).

The last step is consist of the recombination of methylamine-PLP complex and modified γ-vinyl-GABA. The transition structure **09TS10** lies 15.2 kcal mol^{-1} above intermediate **09** with a C8–C12 distance of 2.245 Å (Fig. 8). The relative free energy for the adduct is 1.8 kcal mol^{-1}, which is 5.6 kcal mol^{-1} higher than the Michael addition product.

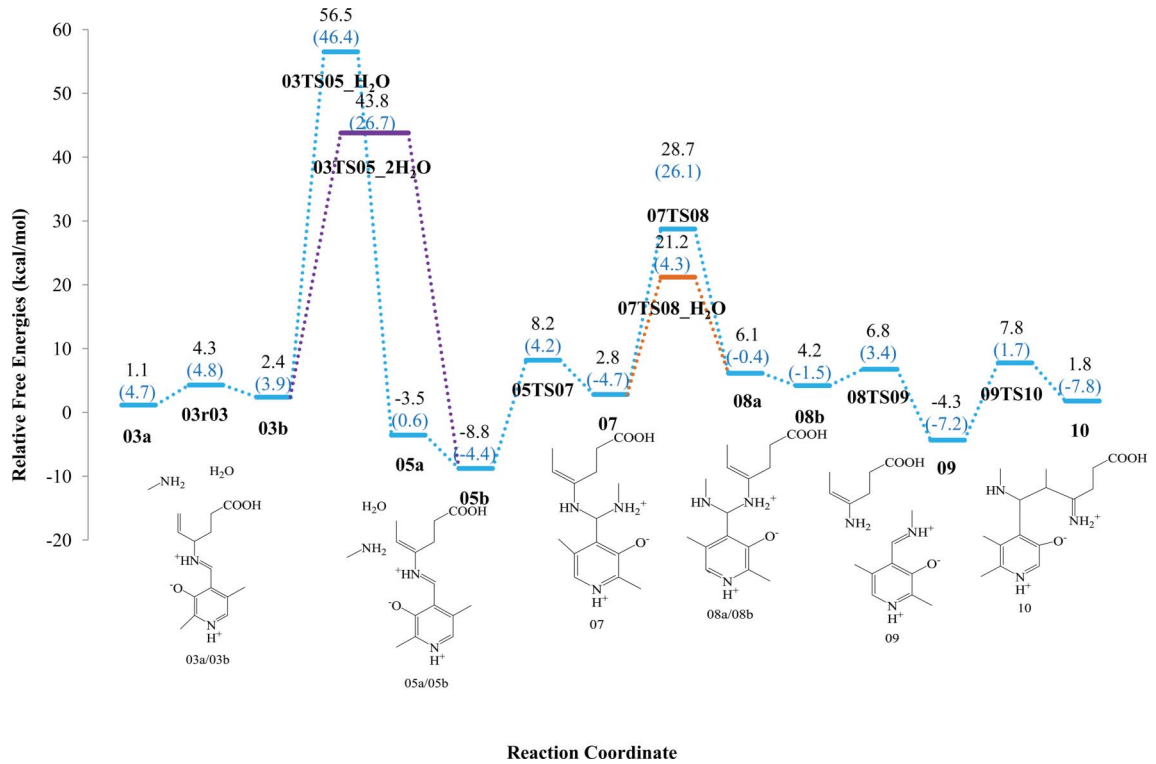

Fig. 7 The reaction profile for the for Enamine pathway (Mechanism 3) in gas phase calculated at B3LYP/6-31+G(d,p) level. Values in parantheses refer to the single point relative energies at the $PCM_{(water)}$/B3LYP/6-31+G(d,p) level of theory.

Energetics of the competing paths

The experimental studies stated that formation of external aldimine is pursued by the three competing paths. Michael addition mechanism is consist of only one step, the activation barrier is highly affected with the presence of both explicit and implicit solvent effect. The activation energy barriers are found to be 40.7 kcal mol^{-1} and 14.8 kcal mol^{-1} for the gas phase and the single point solvent calculations respectively. The activation energy barrier of the Michael addition step in the second mechanism is also substantially decreased by 20 kcal mol^{-1} with the addition of solvent effect (Fig. 5).

Although the allylic isomerization step is a common bottleneck for the two competing Enamine mechanisms, the third mechanism is more likely to occur. The highest activation energy barriers succeding the rate determining step are equal to 12.4 kcal mol^{-1} and 9.0 kcal mol^{-1} for Enamine-Michael and Enamine mechanisms respectively. The differences in the of the product stabilities is also pointed out that the Enamine mechanism is preferable relative to Enamine Michael addition. (Fig. 5 and Fig. 7).

The experimental results also revealed that the Enamine product could be accepted as a minor product with respect to the one obtained from Michael Addition pathway with a ratio of 75 : 25.[19] The rate equation based on the activated complex has yielded the Michael addition:Enamine product ratio to be 70 : 30 in the gas phase which is in line with experimental results. However, when the solvent effect is included the quantitative agreement is not obtained with the experimental ratio. It should be also pointed that in the last experiment conducted by Silverman *et al.*, the enamine product was not detected.[19] Michael addition product is the only detectable product in the experiment. The product distribution was explained by the differences in the thermodynamic stabilities of the two products. We found that the difference between the product stabilities of the two competing paths is equal to 4.9 kcal mol^{-1} approving the Michael addition product. The energy difference between stabilities increased to 11.7 kcal mol^{-1} in the presence of solvent. Hence the solvent effect is the key factor in mechanistic studies related to the enzymatic reactions when model compounds are used.

Conclusion

In this work, inactivation mechanism of GABA-AT in the presence of γ-vinyl-GABA have been studied using the DFT method at the B3LYP/6-31+G(d,p) level of theory, in order to elucidate the preferred inactivation mechanism and to explain the details of the proposed inactivation mechanisms.

The reaction starts with the formation of the external aldimine, which is a common step for all of the proposed inactivation mechanisms. In fact, the external aldimine formation part is essential for the PLP dependent enzymes. The proton transfer step is the rate limiting step both with or without the assistance of explicit water molecules. The decrease in the activation energy barriers due to the solvent effect is mostly experienced by the steps that involve proton relays. The rate determining step turned out to be the first step when the solvent effect is included. After the formation of an external aldimine, there are three pathways to be examined.

The Michael addition can be classified as an asynchronous concerted pathway, where the proton transfer is facilitated by means the nucleophilic attack. The asistance of explicit water

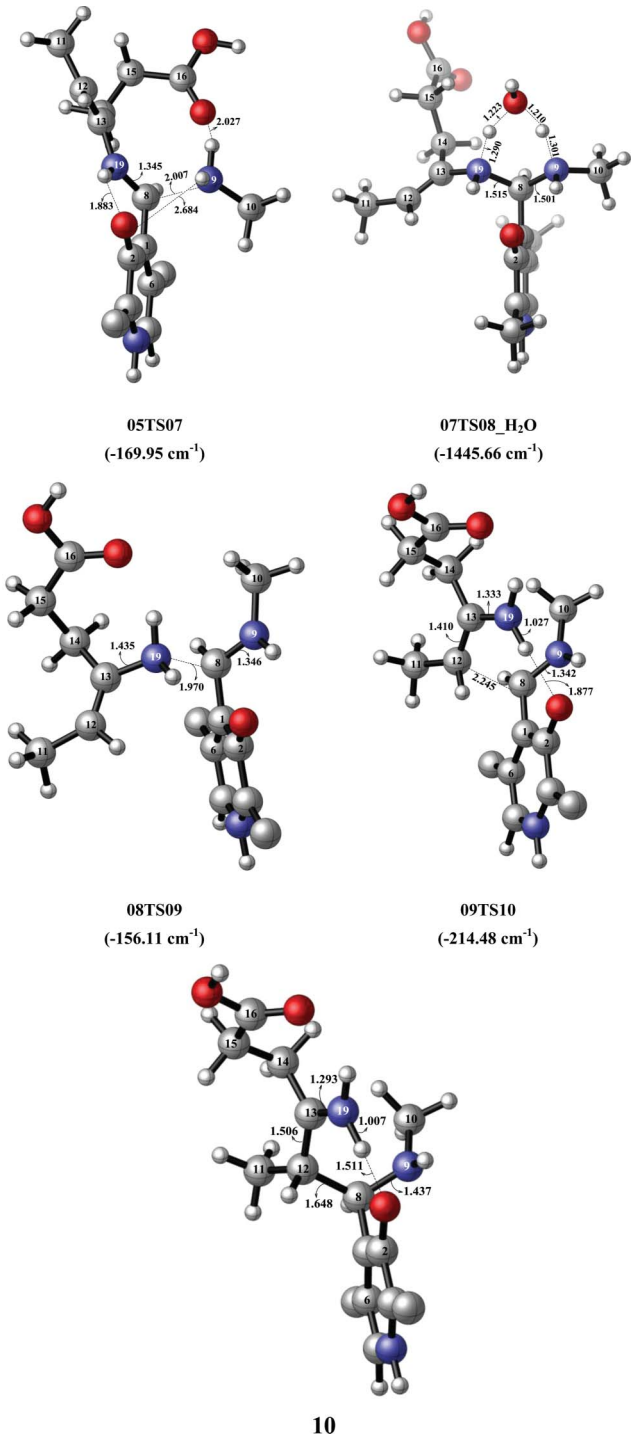

Fig. 8 Three dimensional representations of the stationary points for the Enamine path (Mechanism 3).

molecules decreased the energy barrier about 8 kcal mol^{-1} in gas phase calculations. The decrease in activation energy barrier is found to be 22.3 kcal mol^{-1} when the solvent effect is taken into consideration.

The Enamine-Michael addition is found to be the less probable path among the three based on the product stabilities and energy barriers.

In fact, the reaction involves several proton transfer steps, which are modelled employing a water molecule as a proton acceptor/donor. The energy barriers decreased drastically with the assistance of water molecules. It shoud be pointed out that the activation energies of the proton transfer steps are also affected by such conformational preferences.

As a conclusion, the product obtained after the Michael addition mechanism is thermodynamically more stable relative to Enamine product. In addition, the geometry of the product obtained in the Michael Addition path agrees perfectly with the X-Ray data structure. All the information obtained from the computational studies obviously pointed out that the Michael addition pathway is the preferred mechanism relative to theEnamine pathways.

Acknowledgements

This research was supported by the TUBITAK (Project No: TUB108T344) and the ITU-BAP Thesis project. Computational sources are provided by National High Performance Computing Center at ITU (Grant Number: 20202007) and ITU Informatics Institute. The authors thank Dr Bülent Balta for helpful discussions on solvent entropies.

References

1 J. F. Baxter and E. Roberts, *J. Biol. Chem.*, 1961, **236**, 3287–3294.
2 A. Karlsson, F. Fonnum, D. Malthe-Sorenssen and J. Storm-Mathisen, *Biochem. Pharmacol.*, 1974, **23**, 3053–3061.
3 (*a*) R. A. E. Bakay and A. B. Harris, *Brain Res.*, 1981, **206**, 387–404; (*b*) K. G. Loyd, C. Munati, L. Bossi, C. Stoeffels, J. Talairach and P. L. Morselli, in *Neurotransmission, Seizures, Epilepsy*, P. L. Morselli, W. Loescher and K. G. Loyd, ed., Raven Press: New York, 1981; pp. 325–338; (*c*) J. Butterworth, C. M. Yates and J. J. Simpson, *J. Neurochem.*, 1983, **41**, 440–447; (*d*) N. Nishino, H. Fujiwara, S.-A. Noguchi-Kuno and C. Tanaka, *Jpn. J. Pharmacol.*, 1988, **48**, 331–339; (*e*) T. Aoyagi, T. Wada, M. Nagai, F. Kojima, S. Harada, T. Takeuchi, H. Takahashi, K. Hirokawa and T. Tsumita, *Chem. Pharm. Bull.*, 1990, **38**, 1748–1749.
4 B. S. Meldrum, R. W. Horton, in *Epilepsy*, P. Harris and C. Mawdsley, ed., Churchill Livingston: Edinburgh, 1974; pp 55–64.
5 S. M. Nanavati and R. B. Silverman, *J. Med. Chem.*, 1989, **32**, 2413–2421.
6 (*a*) K. Gale, *Epilepsia*, 1989, **30**, S1–S11, Suppl. 3; (*b*) W. Loscher, *Neuropharmacology*, 1982, **21**, 803–810.
7 G. A. R. Johnston, D. R. Curtis, P. M. Beart, C. J. A. Game, R. M. McColloch and B. J. Twichin, *J. Neurochem.*, 1975, **24**, 157–160.
8 G. A. R. Johnston, A. L. Stephanson and B. J. Twichin, *Pharm. Pharmacol.*, 1977, **29**, 240–241.
9 L. Brehm, H. Hjeds and P. Krogsgarrd-Larsen, *Acta Chem. Scand.*, 1972, **26**, 1298–1299.
10 J. O. McNamara, in *The Pharmacological Basis of Therapeutics*, J. G. Hardman, L. E. Limbird, P. B. Molinoff, R. W. Ruddon and A. G. Gilman, ed., McGraw-Hill: New York, 1996461–486.
11 B. Lippert, B. W. Metcalf, M. J. Jung and P. Casara, *Eur. J. Biochem.*, 1977, **74**, 441–445.
12 B. E. Gidal, M. D. Privitera, R. D. Sheth and J. T. Gilman, *Ann. Pharmacother.*, 1999, **33**, 1277–1286.
13 S. L. Dewey, A. E. Morgan, C. R. Jr. Ashby, B. Horan, S. A. Kushner, J. Logan, N. D. Volkow, J. S. Fowler, E. L. Gardner and J. D. Brodie, *Synapse*, 1998, **30**, 119–129.
14 R. Kalviainen and I. Nousiainen, *CNS Drugs*, 2001, **15**, 217–230.
15 N. Sadlej-Sosnowska, J. Cz. Dobrowolski, W. P. Oziminski and A. P. Mazurek, *J. Phys. Chem. A*, 2002, **106**, 10554–10562.
16 D. De Biase, D. Barra, F. Bossa, P. Pucci and R. A. John, *J. Biol. Chem.*, 1991, **266**, 20056–20061.
17 S. M. Nanavati and R. B. Silverman, *J. Am. Chem. Soc.*, 1991, **113**, 9341–9349.
18 B. W. Metcalf, *Biochem. Pharmacol.*, 1979, **28**, 1705–1712.

19 P. Storici, D. De Biase, F. Bossa, S. Bruno, A. Mozzarelli, C. Peneff, R. B. Silverman and T. Schirmer, *J. Biol. Chem.*, 2004, **279**, 363–373.
20 A. D. Becke, *J. Chem. Phys.*, 1993, **98**, 1372–1377.
21 (*a*) J. J. P. Stewart, *J. Comput. Chem.*, 1989, **10**, 209–220; (*b*) J. J. P. Stewart, *J. Comput. Chem.*, 1989, **10**, 221.
22 Spartan '04, Wavefunction, Inc., 18401 Von Karman Ave., Suite 370, Irvine, CA 92612.
23 M. J. Frisch, G. W. Trucks, H. B. Schlegel, G. E. Scuseria, M. A. Robb, J. R. Cheeseman, J. A. Montgomery, Jr., T. Vreven, K. N. Kudin, J. C. Burant, J. M. Millam, S. S. Iyengar, J. Tomasi, V. Barone, B. Mennucci, M. Cossi, G. Scalmani, N. Rega, G. A. Petersson, H. Nakatsuji, M. Hada, M. Ehara, K. Toyota, R. Fukuda, J. Hasegawa, M. Ishida, T. Nakajima, Y. Honda, O. Kitao, H. Nakai, M. Klene, X. Li, J. E. Knox, H. P. Hratchian, J. B. Cross, V. Bakken, C. Adamo, J. Jaramillo, R. Gomperts, R. E. Stratmann, O. Yazyev, A. J. Austin, R. Cammi, C. Pomelli, J. W. Ochterski, P. Y. Ayala, K. Morokuma, G. A. Voth, P. Salvador, J. J. Dannenberg, V. G. Zakrzewski, S. Dapprich, A. D. Daniels, M. C. Strain, O. Farkas, D. K. Malick, A. D. Rabuck, K. Raghavachari, J. B. Foresman, J. V. Ortiz, Q. Cui, A. G. Baboul, S. Clifford, J. Cioslowski, B. B. Stefanov, G. Liu, A. Liashenko, P. Piskorz, I. Komaromi, R. L. Martin, D. J. Fox, T. Keith, M. A. Al-Laham, C. Y. Peng, A. Nanayakkara, M. Challacombe, P. M. W. Gill, B. Johnson, W. Chen, M. W. Wong, C. Gonzalez and J. A. Pople, *Gaussian 03, (Revision D.01)*, Gaussian Inc, Wallingford CT, 2004.
24 A. E. Reed, L. A. Curtiss and F. Weinhold, *Chem. Rev.*, 1988, **88**, 899–926.
25 (*a*) M. Cossi, V. Barone, R. Cammi and J. Tomasi, *Chem. Phys. Lett.*, 1996, **255**, 327–335; (*b*) V. Barone, M. Cossi and J. Tomasi, *J. Comput. Chem.*, 1998, **19**, 404–417; (*c*) M. Caricato, F. Ingrosso, B. Mennucci and J. Tomasi, *J. Chem. Phys.*, 1999, **122**, 154501–154510.
26 R.-Z. Liao, W.-J. Ding, J.-G Yu, W.-H Fang and R.-Z Liu, *J. Comput. Chem.*, 2008, **29**, 1919–1929.
27 R. Casasnovas, A. Salva, J. Frau, J. Donoso and F. Munoz, *Chem. Phys.*, 2009, **355**, 149–156.
28 R. D. Bach, C. Canepa and M. N. Glukhovtsev, *J. Am. Chem. Soc.*, 1999, **121**, 6542–6555.
29 (*a*) M. D. Toney, *Arch. Biochem. Biophys.*, 2005, **433**, 279–287; (*b*) M. D. Toney, *Biochemistry*, 2001, **40**, 1378–1384.
30 S. Sharif, G. S. Denisov, M. D. Toney and H. H. Limbach, *J. Am. Chem. Soc.*, 2007, **129**, 6313–6327.
31 (*a*) A. Salvà, J. Donoso, J. Frau and F. Muñoz, *J. Phys. Chem. A*, 2003, **107**, 9409–9414; (*b*) A. Salvà, J. Donoso, J. Frau and F. Muñoz, *J. of Mol. Struct. (THEOCHEM)*, 2002, **577**, 229–238.
32 (*a*) A. Salvà, J. Donoso, J. Frau and F. Muñoz, *J. Phys. Chem. A*, 2004, **108**, 11709–11714; (*b*) A. Salvà, J. Donoso, J. Frau and F. Muñoz, *Int. J. Quantum Chem.*, 2002, **89**, 48–56.
33 C. Y. Legault, *CYLview*, 1.0b, Université de Sherbrooke, 2009 (http://www.cylview.org).
34 R.-Z. Liao, W.-J. Ding, J.-G. Yu, W.-H. Fang and R.-Z. Liu, *J. Phys. Chem. A*, 2007, **111**, 3184–3190.
35 L. Pardo, R. Osman, H. Weinstein and J. R. Rabinowitz, *J. Am. Chem. Soc.*, 1993, **115**, 8263–8269.
36 M. P. Patil and R. B. Sunoj, *J. Org. Chem.*, 2007, **72**, 8202–8215.
37 J. Ortega-Castro, M. Adrover, J. Frau, A. Salva, J. Donoso and F. Munoz, *J. Phys. Chem. A*, 2010, **114**, 4634–4640.
38 J. J. Likos, H. Ueno, R. W. Feidhaus and D. E. Metzler, *Biochemistry*, 1982, **21**, 4377–4386.
39 H. Ueno, J. J. Likos and D. E. Metzler, *Biochemistry*, 1982, **21**, 4387–4393.